Available online at www.sciencedirect.com
SCIENCE DIRECT®
Optics Communications 245 (2005) 301–308
OPTICS COMMUNICATIONS
www.elsevier.com/locate/optcom

Transverse excess noise factor and transverse mode locking in a gain-guided laser

Ching-Hsu Chen [a,*], Po-Tse Tai [b], Wei-How Chiu [b], Wen-Feng Hsieh [b,*]

[a] National Center for High-Performance Computing, 21 Nan-Ke 3rd Rd., Hsinshi, Tainan County 744, Taiwan
[b] Department of Photonics and Institute of Electro-Optical Engineering, National Chiao Tung University, 1001 Tahsueh Rd., Hsinchu 30050, Taiwan

Received 30 May 2004; received in revised form 27 August 2004; accepted 1 October 2004

Abstract

We use the Collins integral together with a rate equation to calculate the transverse mode profiles near $g_1g_2 = 1/4$ in a tightly focused end-pumped Nd:YVO_4 laser. The transverse mode locking is confirmed from the mode decomposition into the degenerate empty-cavity eigenmodes and from the observation of beam profile variation along the propagation distance. We obtain that the calculated transverse excess noise factor without considering the thermal effect is consistent with the previous research and it depends on the pump size. We further study the influence of the thermal lens effect on the K factor and discuss how to suppress the laser instabilities that occur near the degeneracy.

PACS: 42.60.Jf; 42.60.Da; 42.50.Lc; 42.55.Xi
Keywords: Beam characteristics; Resonators; Diode-pumped lasers

1. Introduction

The excess noise factor was discussed first by Petermann [1] in a gain-guided semiconductor laser and thus it is called Petermann K factor. The K factor is large in unstable laser cavities due to non-orthogonality properties of the transverse modes [2,3]. In the case of a geometrically stable cavity, introducing apertures inside the cavity was shown leading to large K factors [4]. Recently, Maes and Wright [5] found that the K factor is cavity-configuration-dependent near the degenerate cavity configurations in a geometrically stable cavity with Gaussian gain. They explained that $K = 1$ at the exact degeneracies is due to flat phase front coming from the phase-locked empty-cavity eigenmodes and that a large value of K beside

* Corresponding authors. Tel.: +88 665 724 805; fax: +88 635 716 631.
E-mail addresses: q1410928@ms38.hinet.net (C.-H. Chen), wfhsieh@mail.nctu.edu.tw (W.-F. Hsieh).

0030-4018/$ - see front matter © 2004 Elsevier B.V. All rights reserved.
doi:10.1016/j.optcom.2004.10.003

the degeneracies is due to highly curved phase front resulting from the incoherent superposition of the empty-cavity eigenmodes.

Previously, we have observed the multi-beam-waist (MBW) modes [6] near the degenerate cavity of $g_1g_2 = 1/4$ in a tightly focused end-pumped Nd:YVO_4 laser. Our laser system that consists of a plano-concave cavity with the flat end mirror at the coated face of the Nd:YVO_4 crystal is the same as that of in [5]. We have understood the MBW mode at the exact degeneracy by a combination picture of ray and wave optics that is similar to the notation of the asymmetric modes [7]. Furthermore, in the same system the cavity-configuration-dependent laser instabilities were found on each side of the degeneracy of $g_1g_2 = 1/4$ and the thermal lens effect induced by the tightly focused pump were considered to explain the experimental data [8]. Because the thermal lens effect introduces a phase distribution into the diffraction, it will influence the transverse mode and the K factor. Therefore, it is necessary to include the thermal lens effect in the calculation of K factor. Moreover, the laser instabilities appear near the region of maximal K factor for some conditions, so the laser parameters should be chosen carefully when one wants to measure the K factor in such a laser.

In this work, we use the Collins integral together with a rate equation to calculate the transverse mode profiles near $g_1g_2 = 1/4$. We further use the genetic algorithm (GA) to decompose the calculated mode profile into the degenerate Laguerre–Gaussian (LG) modes and thus obtain their mode weightings and relative phases. Most importantly, from the experimental observation of beam profile variation along the propagation distance, we confirm phase-locking of the degenerate transverse modes near the degeneracy. We calculate the K factor with and without considering the thermal effect and obtain that it is not only cavity-configuration-dependent but also pump-size-dependent. In Section 2, we describe the mode-calculation model including the thermal lens effect. In Section 3.1, we show the numerical results of mode calculation together with the fitted mode expansion and then show the mode profile variation along propagation distance. The K factor as a function of the cavity length is studied in Section 3.2 with and without considering the thermal lens effect. The laser instabilities are also discussed. The conclusions are stated in Section 4.

2. The calculation model

Consider a plano-concave end-pumped solid-state laser shown in Fig. 1. It consists of a laser crystal with one of its end faces high-reflection coated as a flat mirror and of a curved mirror with radius of curvature R, which are separated by distance L. Let the reference plane be the place where the light beam just leaves the laser crystal toward the curved mirror. Under cylindrical symmetry, propagation of the light field toward the curved mirror and back to the flat mirror according to the Collins integral is [9]

$$E^-_{m+1}(r) = \frac{-2\pi \mathrm{i}}{B\lambda}\int_0^a \exp(\mathrm{i}k2L)E^+_m(r') \times \exp\{(\mathrm{i}\pi/B\lambda)(Ar'^2 + Dr^2)\} \times J_0(2\pi rr'/B\lambda)r'\,\mathrm{d}r', \quad (1)$$

with round trip transmission matrix $\begin{bmatrix} A & B \\ C & D \end{bmatrix}$. Here $E^+_m(r')$ and $E^-_{m+1}(r)$ are the electric fields of the mth and the $(m+1)$th round trips, respectively, at the planes immediately after and before the gain medium (denoted by the superscripts + and −); r' and r are the corresponding radial coordinates, λ is the wavelength of the laser, a is the aperture radius on the reference plane, and J_0 is a Bessel function of zero order. The aperture radius must be chosen large enough with many times of the fundamental mode radius to ensure that the diffraction loss can be neglected. In a thin-slab approximation, we can relate the electric fields E^+_{m+1} to E^-_{m+1} (after and before the gain medium) in the same round trip as

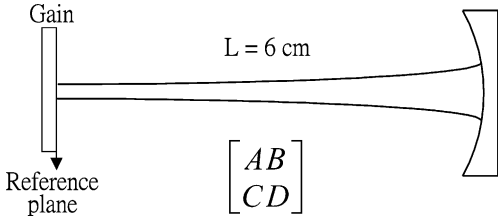

Fig. 1. Configuration of the laser system.

$$E^{+}_{m+1}(r) = \rho E^{-}_{m+1}(r)\exp(\sigma \Delta N d)\Pi(r/a), \tag{2}$$

where $1-\rho^2$ is the round-trip energy loss, σ is the stimulated-emission cross-section, ΔN is the population inversion per unit volume, d is the length of the active medium, and $\Pi(r/a)$ is an aperture function that equals 1 for r less than aperture radius a and equals 0 otherwise. Furthermore, assuming that the evolution of the population inversion follows the rate equation of a four-level system, we can write the rate equation as

$$\Delta N_{m+1} = \Delta N_m + R_{\mathrm{pm}}\Delta t - \gamma \Delta N_m \Delta t - \frac{|E_m|^2}{E_s^2}\Delta N_m \Delta t, \tag{3}$$

where R_{pm} is the pumping rate, Δt is the round-trip time, E_s is the saturation parameter of the active medium, and γ is the spontaneous decay rate. It was found that a standing-wave resonator can be approximated by a ring resonator if a thin gain medium is placed close to one of the end mirrors [10]. This method is similar to the Fox–Li approach [11] and has been used to analyze the decay rate of standing-wave laser cavities [12]. For a continuous Gaussian pump profile $R_{\mathrm{pm}} = R_{\mathrm{p0}}\exp(-2r^2/w_{\mathrm{p}}^2)$ with constant pump beam radius w_{p} throughout the active medium (thin slab), the total pump rate over the entire active medium is

$$\int_V R_{\mathrm{pm}}\,\mathrm{d}V = P_{\mathrm{p}}/h\nu_{\mathrm{p}}, \tag{4}$$

where P_{p} is the effective pump power and $h\nu_{\mathrm{p}}$ is the photon energy of the pumping laser. Because we concerned chiefly with transverse mode profile, we did not consider the dispersion of the active medium or frequency detuning between the atomic transition and the cavity mode; thus the gain was assumed to be real. When the thermal lens effect was considered, we imposed a term $\exp(-\mathrm{i}\Delta\Phi(r))$ in the diffraction integral, where $\Delta\Phi(r)$ is the phase shift induced by thermal lens effect. According to Eqs. (2), (6), and (11) of [13], the phase shift can be written as

$$\Delta\Phi(r') = \int_0^d k\Delta T(r',z)\frac{\mathrm{d}n}{\mathrm{d}T}\,\mathrm{d}z, \tag{5}$$

where

$$\Delta T(r',z) = -\frac{1}{Kc}\int_{r'}^{r_b}\frac{\alpha\xi P_{\mathrm{abs}}}{2\pi}\exp(-\alpha z) \times \frac{1-\exp(-2r^2/w_{\mathrm{p}}^2)}{r}\,\mathrm{d}r$$

is the temperature difference between the calculated point (r',z) and the boundary point (r_b,z), w_{p} is the pump radius, ξ is the fractional thermal loading, P_{abs} is the absorbed pump power, z is the axial coordinate, and r_b, d, α, K_c, and $\mathrm{d}n/\mathrm{d}T$ are the radius, thickness, absorption coefficient, thermal conductivity, and the thermal-optic coefficient of the laser crystal, respectively. The thermal induced stress, the thermal deformation of the crystal, and the thermal fluctuation were neglected.

In an ordinary axially pumped solid-state laser, the round-trip propagation time is many orders of magnitude shorter than the spontaneous decay time, especially in a short cavity; as a result, it would take a large number of iterations to arrive at the convergent state. To reduce computation time, we used the scaling method [12] to magnify the γ value of the Nd:YVO_4 laser by 100 times to obtain the continuous-wave solution because the transverse mode distribution is independent of γ as long as $\Delta t \ll 1/\gamma$. Given an initial ΔN and E, after the power output undergoes a procedure similar to the relaxation oscillation the field distribution E converges to a cw steady solution. In our simulation, the aperture was chosen 600 μm that is much larger than the fundamental beam radius of 108 μm for $g_1g_2 = 1/4$. To implement the Collins integral by the Romberg method, we divided the 600-μm aperture radius into 1024 segments.

3. Results and discussion

3.1. Transverse mode locking

The parameters used for mode calculation are the same as in [6]. The important control parameters in this work are the cavity length L and the pump radius w_{p}. The other parameters for calculating the thermal lens effect are $\xi = 0.23$, $\alpha = 1930\ \mathrm{m}^{-1}$, $K_c = 5.23\ \mathrm{W\,m^{-1}\,K^{-1}}$, and $\mathrm{d}n/\mathrm{d}T = 8.5\times10^{-6}\ \mathrm{K}^{-1}$. We show the normalized intensity profile and

the phase profile on the reference plane with solid circles in Figs. 2(a) and (b) at the degeneracy (L = 6 cm) for w_p = 30 μm and the effective pump power of 100 mW without considering the thermal lens effect. In order to show the good fitting of mode decomposition using GA, we plot the fitted results in Figs. 2(a)–(d) with open circles and use the logarithm scale in Fig. 2(a). The mode decomposition is done with 13 fitting parameters including six amplitude weightings and seven relative phases. For the aperture radius of 600 μm on the reference plane, we expand the calculated mode profile into the 1/3-degenerate LG_{pm} modes with $p = 0, 3, 6, \ldots, 18$ and $m = 0$, where p is the radial mode index and m is the angular index. The normalized electric field of LG_{p0} mode can be expressed as

$$E_{p0}(r,z) = A_{p0}(r,z)\exp\left(-\frac{r^2}{w(z)^2}\right)\exp\left(i\frac{kr^2}{2R(z)}\right) \times \exp\left\{i\left[kz-(2p+1)\tan^{-1}\left(\frac{z}{z_R}\right)+\delta_p\right]\right\},$$

where

$$A_{p0}(r,z) = E_0\frac{w_c}{w(z)}L_p^0\left(\frac{2r^2}{w(z)^2}\right)$$

is the modal function, E_0 is the normalization constant, z_R is the Rayleigh length, $w(z)$ is the beam

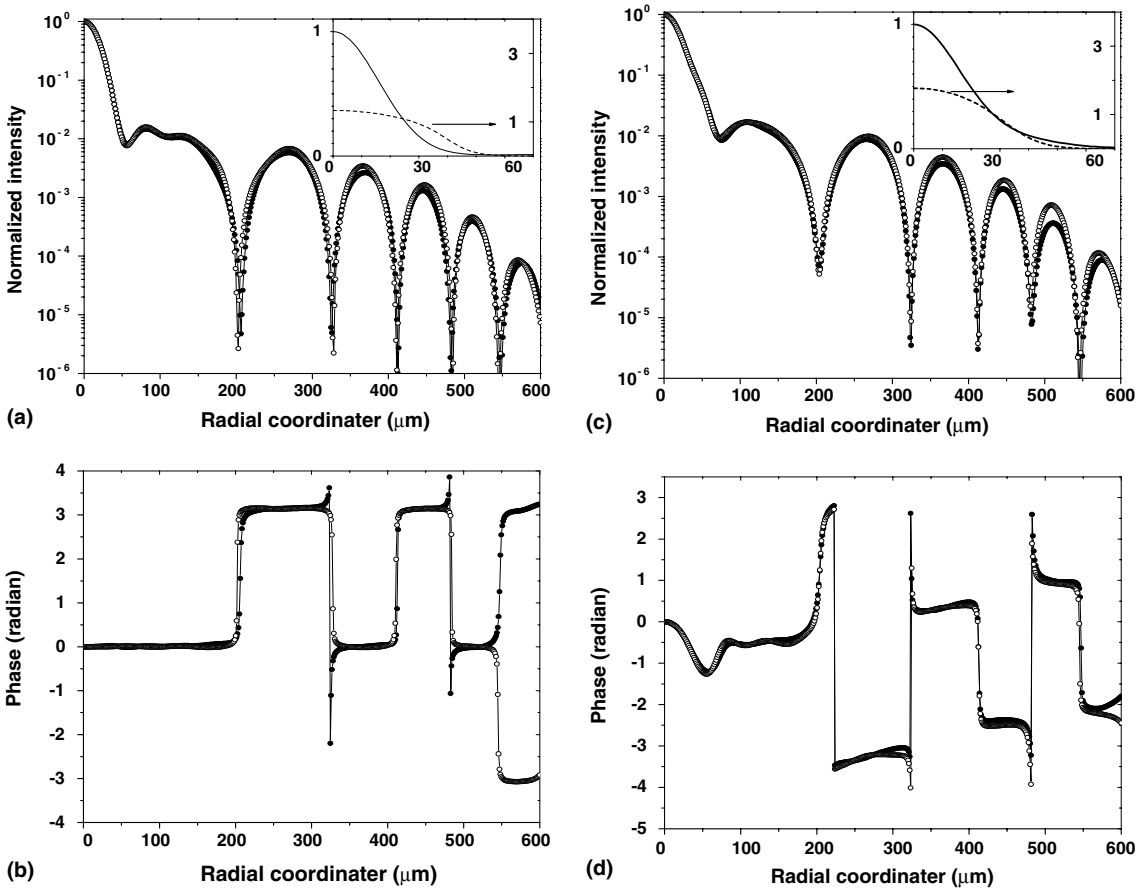

Fig. 2. The intensity profile in logarithm scale (a) and the phase profile (b) at the exact degeneracy (L = 6.0 cm) obtained from the mode calculation (solid circles) and from the fitted result of mode decomposition (empty circles). Inset in (a) are the intensity profile in linear scale (solid curve) and the saturated gain distribution (dashed curve). (c) and (d) are, respectively, the intensity and phase profiles for L = 6.01 cm.

radius, $R(z)$ is the radius of curvature of the phase front, r and z are, respectively, the radial and axial coordinates, and L_p^0 is the Laguerre polynomial for mode index p. We assume all the excited LG_{p0} modes have the same wavenumber and then the intensity profile $|\eta_0 E_{00} + \eta_3 E_{30} + \cdots + \eta_{18} E_{18,0}|^2$ with seven amplitude weightings $\eta(\eta_0$ be fixed unity) and seven relative phases δ_p is fitted to the mode-calculation profile. We see that the resultant fitted profiles match with the mode-calculation profiles extremely well in Figs. 2(a)–(d). From Fig. 2(a) the central lobe of the intensity profile is near-Gaussian with the waist radius of ~30 μm (approximately equals to the pump radius, see the solid curve in the inset with linear scale), which shows that the laser is strongly gain-guided. Note that the radius of the fundamental mode, w_o, is 108 μm. The seriously saturated gain distribution is shown with the dashed curve in the inset of Fig. 2(a). The gain distribution is obtained from the term $\exp(\sigma \Delta N d)$ in Eq. (2), where ΔN is r-dependent. Fig. 2(b) shows that the phase profile is flat within $r = 200$ μm but discontinuously jumps π phase at some positions of r, e.g., the first phase jump at $r = 200$ μm corresponds to the position of the second intensity zero of the $LG_{3,0}$ mode. The relative phases of the degenerate LG modes for $L = 6.0$ cm show the degenerate LG modes are not only phase-locked but also nearly in-phase on the reference plane. The unusual result of flat wavefront on the flat end mirror, obtained in our mode calculation including gain, is the same as in [5] and this was discussed therein.

When the cavity length is slightly tuned away from the degeneracy to $L = 6.01$ cm, the central lobe of the intensity profile shows a slightly distorted Gaussian in the inset of Fig. 2(c) with the solid curve in linear scale. Also shown with the dashed curve in the inset is the saturated gain distribution. We can see in Fig. 2(d) that the phase pattern is already highly curved for $r < 100$ μm and no longer has π-jumps at some positions of r. Note that the phase is continuous at $r = 223$ μm because the phase jump is 2π. Besides, at $L = 6.01$ cm the degenerate LG_{p0} modes are no longer in-phase on the reference plane but have monotonically increasing relative phases with the increase of p. Even so, these LG_{p0} modes are still phase-locked to form a stationary mode. Such a stationary mode exhibits profile variation along the propagation distance due to the variation of Gouy phases of the LG_{p0} modes and it is in fact an optical bottle beam that has been presented in [14]. It is worthy to note that nearly the same behavior for the case of $L = 5.99$ cm except that the phase pattern is inverted within $r = 100$ μm and the relative phases of the LG_{p0} modes decrease monotonically with increase of p.

At $L = 6.05$ cm, the intensity profile is much distorted from Gaussian and the phase pattern is highly curved for $r < 150$ μm. We will show later that this cavity length corresponds to where the maximal K factor is. The mode weightings and the relative phases of the LG_{p0} modes for various cavity lengths are summarized in Figs. 3(a) and (b) except for the absence of $L = 6.04$ cm because the laser instability occurs there. The self-pulsing and chaotic time evolution have been observed there and also on the other side of the degeneracy when the pump radius is smaller than 40 μm [8]. We can see in Fig. 3 that the mode weightings for the case of $L = 6.05$ cm have significant decrease for $p = 3$, 6, 9 as compared with the case of $L = 6.03$ cm and that the relative phases no longer monotonically increase but alternate for $p > 6$.

Although the far-field intensity pattern looks like a Gaussian profile when the cavity is tuned far away from the degeneracy to $L = 6.10$ cm, the mode profile still varies along the propagation. We can see from Fig. 4(a) that the calculated mode profile exhibits a dark center from $z = 6.8$ to 8.0 cm. We therefore used this z-dependent profile to verify the phase-locking of degenerate transverse modes as L is tuned from 5.90 to 6.10 cm. The profile will appear a dark center approximately from 19 to 23 cm after a convergent lens with focal length of 7 cm when the convergent lens is put behind the output coupler at a distance of 12 cm. Fig. 4(b) shows the photograph taken at a distance of 20.5 cm after the convergent lens from our Nd:YVO_4 laser as L is set on the right edge of the phase-locking region. We found experimentally that the phase-locking region has been shifted ~500 μm toward the short cavity side by the thermal lens effect for $w_p = 30$ μm and pump power of 150 mW.

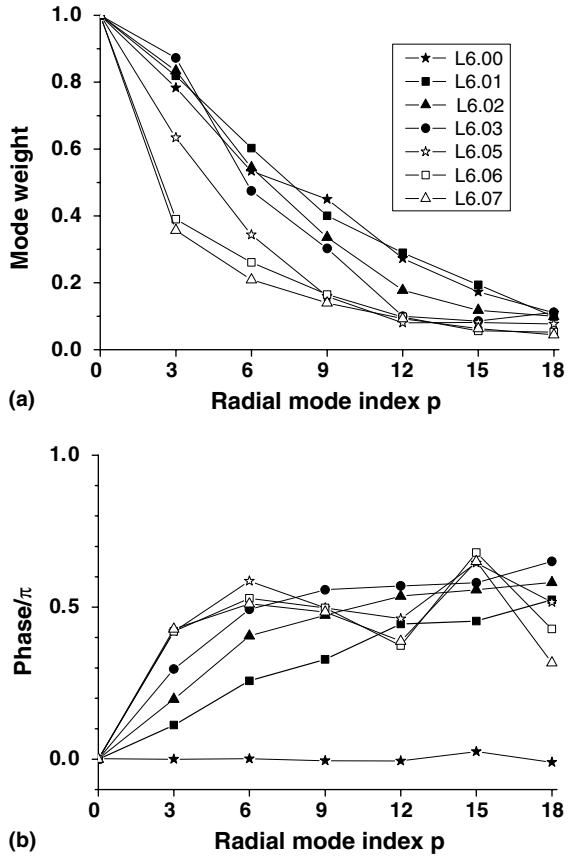

Fig. 3. The mode weightings (a) and the relative phases (b) of the LG_{p0} modes as L is tuned away from the degeneracy.

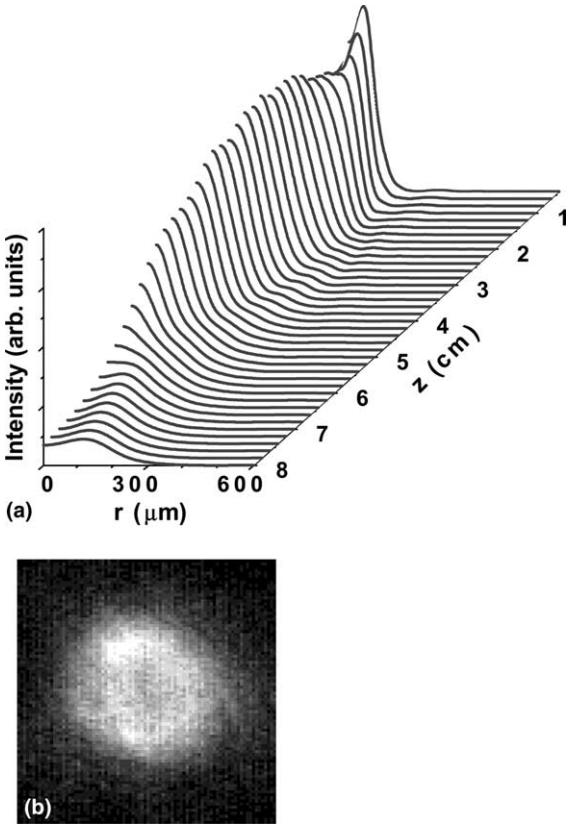

Fig. 4. (a) The numerical beam profile variation along the propagation distance z for $L = 6.10$ cm. The intensity profile with a dark center can be seen at $z = 6.8-8.0$ cm that is transformed to a distance of 19–23 cm after the convergent lens. (b) The photograph experimentally taken at 20.5 cm after the convergent lens.

3.2. Transverse excess noise factor

We calculate the K factor according to the relation given by [4,5], $K = [\int_0^\infty |E(r)|^2 r\,dr]^2 / |\int_0^\infty E^2(r) r\,dr|^2$, that is valid for a plano-concave cavity with the electric field $E(r)$ at the flat end mirror [5]. The upper limit of the integral in the expression of K may be replaced by the aperture radius as long as the aperture radius is large enough. Our calculation shows that the K factor is indeed independent of the aperture radius for a convergent solution $E(r)$ except for $L = 6.04$ cm where the laser instability appears. Thus, the variation of K factor shown below does not result from diffraction via the aperture [4] but from the inherent mode properties [5] near the degenerate cavity.

By decreasing the aperture radius on the reference plane from 600 down to 500 μm, we found that the K factor is unchanged for the stable output but the laser instabilities (e.g., $L = 6.04$ cm) are suppressed. Fig. 5(a) shows the K factor as a function of L for $w_p = 40$ μm with solid triangles and $w_p = 30$ μm with solid circles when the aperture radius is 500 μm without considering the thermal lens effect. We obtain that the K factor is pump-size-dependent besides cavity-configuration-dependent. However, further decreasing the pump size smaller than 30 μm does not increase the K factor. It seems that there is a proper pump size that leads to the largest K-factor. For comparing the value of K with the results of [5] around

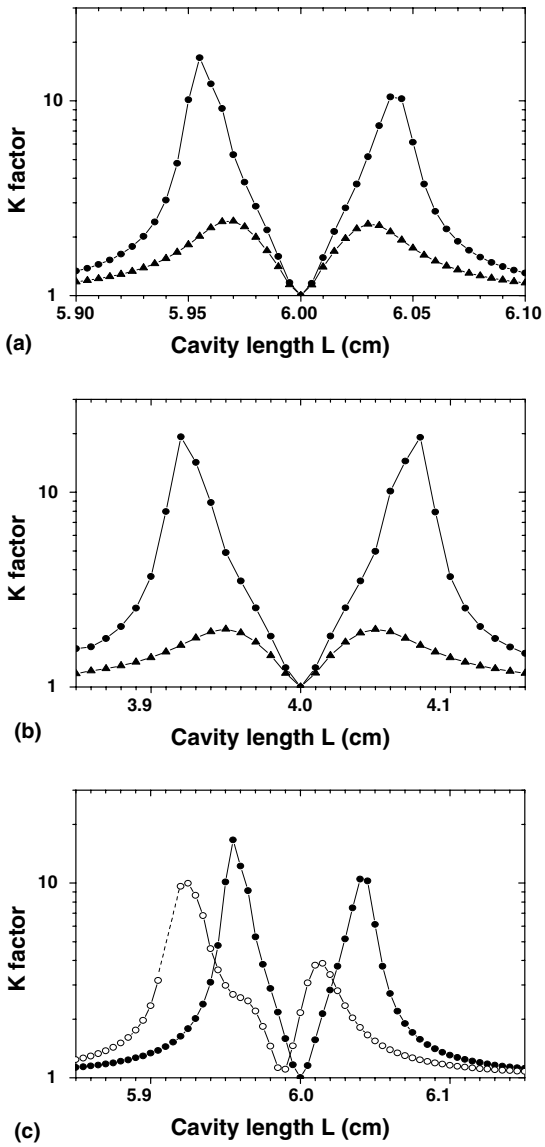

Fig. 5. (a) The K factor as a function of L for $w_p = 30$ μm (solid circles) and 40 μm (solid triangles) near $g_1g_2 = 1/4$ without considering the thermal lens effect. (b) The cavity-dependent K factor for $w_p = 40$ μm (solid circles) and 58 μm (solid triangles) near $g_1g_2 = 1/2$ without considering the thermal lens effect. Note that $w_o = 116$ μm for $L = 4$ cm near $g_1g_2 = 1/2$. (c) The cavity-dependent K factor for $w_p = 30$ μm and the effective pump power of 100 mW near $g_1g_2 = 1/4$ with (open circles) and without (solid circles) considering the thermal lens effect.

$g_1g_2 = 1/2$, we calculated two cases of $w_p = 58$ μm ($w_p/w_o = 1/2$, solid triangles) and $w_p = 40$ μm (solid circles) in Fig. 5(b). The case of $w_p = 58$ μm is consistent with Fig. 2 of [5]. The value of K factor is comparable for $w_p = 30$ μm in Fig. 5(a) and for $w_p = 40$ μm in Fig. 5(b) that means the degeneracy of $g_1g_2 = 1/4$ is also a good choice for measuring the cavity-configuration-dependent K factor.

As aforementioned, a proper small pump size results in large K but it may lead to the instabilities and strengthen the thermal lens effect. Because the thermal lens effect introduces a phase distribution into the electric field, in turn it will influence the K factor. When the thermal lens effect is included, the result plotted as open circles in Fig. 5(c) shows that the K-curve of $w_p = 30$ μm is shifted and distorted from the feature of without the thermal lens effect. Also, the K-factor is decreased by the thermal lens effect. When the thermal lens effect is considered, the laser instabilities occur at $L \sim 5.91$ cm that is shifted from $L \sim 5.96$ cm without considering the thermal lens effect. Further decreasing the aperture radius to 450 μm is able to fully suppress the laser instabilities. In experiment, decreasing the aperture may be achieved by focusing the pumping beam near the rim of the crystal instead of setting a real hard aperture against the crystal inside the cavity. It is worthy to note that the instabilities are also found near the degeneracy of $g_1g_2 = 1/2$, for which the instability occurs at $L = 3.91$–3.94 cm and $L = 4.06$–4.09 cm for $w_p = 40$ μm when the aperture radius is larger than 500 μm. Therefore, the laser parameters must be chosen carefully for measuring the cavity-configuration-dependent K factor near the degeneracies.

4. Conclusion

We have confirmed the phase-locking of degenerate transverse modes near the degeneracy of $g_1g_2 = 1/4$ in a tightly focused end-pumped Nd:YVO_4 laser that can be verified by observation of beam profile variation along the propagation distance within a large cavity-length detuning from the degeneracy. We also decomposed the stationary lasing mode into the degenerate Laguerre–Gaussian modes with their relative locked phase. Furthermore, we obtained that the K factor is cavity-configuration-dependent and pump-size-dependent. When the thermal lens effect is taken

into account the cavity-configuration-dependent K factor is shifted and decreased. Although the laser instabilities appear near the region of maximal K factor they can be suppressed.

Acknowledgment

The research was partially supported by the National Science Council of the Republic of China under Grant NSC93-2112-M-009-035.

References

[1] K. Pertermann, IEEE J. Quantum Electron. 15 (1979) 566.
[2] A.E. Siegman, Phys. Rev. A 39 (1989) 1264.
[3] Y.J. Chen, C.G. Fanning, A.E. Siegman, Phys. Rev. Lett. 77 (1996) 627.
[4] M. Brunel, G. Ropars, A.L. Floch, F. Bretenaker, Phys. Rev. A 55 (1997) 4563.
[5] C.F. Maes, E.M. Wright, Opt. Lett. 29 (2004) 229.
[6] C.H. Chen, P.T. Tai, M.D. Wei, W.F. Hsieh, J. Opt. Soc. Am. B 20 (2003) 1220.
[7] W.J. Firth, Opt. Commun. 22 (1977) 226.
[8] C.H. Chen, P.T. Tai, W.F. Hsieh, Opt. Commun. 241 (2004) 145.
[9] S.A. Collins, J. Opt. Soc. Am. 60 (1970) 1168.
[10] M. Moller, L.M. Hoffer, G.L. Lippi, T. Ackemann, A. Gahl, W. Lange, J. Mod. Opt. 45 (1998) 1913.
[11] A.G. Fox, T. Li, IEEE J. Quantum Electron. 2 (1966) 774.
[12] Y.J. Cheng, P.L. Mussche, A.E. Siegman, IEEE J. Quantum Electron. 31 (1995) 391.
[13] M.E. Innocenzi, H.T. Yura, C.L. Fincher, R.A. Field, Appl. Phys. Lett. 56 (1990) 1831.
[14] C.H. Chen, P.T. Tai, W.F. Hsieh, Appl. Opt. (to be published).